Unique physiology of Lepisosteidae imparts a novel phosphate-water fractionation in their scale biogenic apatite

Katelyn Gray[1], Mark Brandon[2], and Ruth Blake[2]

[1]University of Delaware
[2]Yale University

November 23, 2022

Abstract

Determining paleotemperatures in terrestrial environments are much more challenging than those in the ocean because of stratigraphic inconsistencies, strong spatial and temporal variations in temperature, and a paucity of well-tested methods. Here we utilize the ganoine scales of gars from the family Lepisosteidae to calibrate a new terrestrial paleothermometer. Gars are widespread both in the modern and in the past, as they are a freshwater fish lineage that extends back into the Cretaceous (100 Ma) and have remained relatively unchanged during that time span. Gars constantly record water temperatures, whose yearly average is closely related to mean annual temperature, in their body tissues, including scales. These scales grow continuously throughout life, are >95% hydroxyapatite and thus are highly resistant to diagenetic alteration. Oxygen isotopes in both biogenic phosphates and carbonates have been used to reconstruct environments on land with varying degrees of success. Phosphate-oxygen isotopes are more resistant to post-mortem alteration as the phosphorus-oxygen bond is stronger than the carbon-oxygen bond. We investigate the application of phosphate oxygen isotopes to gar scales by collecting scales from modern individuals from a north-south transect across the United States, exploiting the latitudinal temperature gradient in mean annual temperatures, measuring δ18Ophosphate of those scales, and comparing these values to the average δ18Owater and temperature of each locality. We compare our δ18Ophosphate calibration to previously published curves. Our work demonstrates that the δ18Ophosphate values of gar scales are robust recorders of temperature and δ18Owater.

Unique physiology of Lepisosteidae imparts a novel phosphate-water fractionation in their scale biogenic apatite

Katelyn E. Gray[a*], Ruth E. Blake[a], and Mark T. Brandon[a]

[a] Department of Geology and Geophysics, Yale University, New Haven, CT 06511, United States

* Corresponding author: Katelyn E. Gray, (katelyn.gray@aya.yale.edu)

Present address**:** Department of Plant and Soil Sciences, University of Delaware, 221 Academy St, Newark, DE 19716

Keywords: bioapatite; gar; phosphate; oxygen isotopes; paleotemperature

Declarations of Interest: None

Abstract

Determining paleotemperatures in terrestrial environments are much more challenging than those in the ocean because of stratigraphic inconsistencies, strong spatial and temporal variations in temperature, and a paucity of well-tested methods. Here we utilize the ganoine scales of gars from the family Lepisosteidae to calibrate a new terrestrial paleothermometer. Gars are widespread both in the modern and in the past, as they are a freshwater fish lineage that extends back into the Cretaceous (100 Ma) and have remained relatively unchanged during that

time span. Gars constantly record water temperatures, whose yearly average is closely related to mean annual temperature, in their body tissues, including scales. These scales grow continuously throughout life, are >95% hydroxyapatite and thus are highly resistant to diagenetic alteration.

Oxygen isotopes in both biogenic phosphates and carbonates have been used to reconstruct environments on land with varying degrees of success. Phosphate-oxygen isotopes are more resistant to post-mortem alteration as the phosphorus-oxygen bond is stronger than the carbon-oxygen bond. We investigate the application of phosphate oxygen isotopes to gar scales by collecting scales from modern individuals from a north-south transect across the United States, exploiting the latitudinal temperature gradient in mean annual temperatures, measuring $\delta^{18}O_{phosphate}$ of those scales, and comparing these values to the average $\delta^{18}O_{water}$ and temperature of each locality. We compare our $\delta^{18}O_{phosphate}$ calibration to previously published curves. Our work demonstrates that the $\delta^{18}O_{phosphate}$ values of gar scales are robust recorders of temperature and $\delta^{18}O_{water}$.

1. Introduction

Our understanding of Earth's climatic history is dominated by the interpretation of oceanic sediments, which lacks sensitivity to the climate of continental interiors. Terrestrial paleoclimate knowledge comes from well-preserved plant remains, fossils, speleothems, paleosols, and lacustrine and riverine sediments. Lakes and streams are known to closely match atmospheric air temperature, as they are about 1 °C warmer over the course of a year (e.g. Fricke and Wing, 2004). As ectotherms with indeterminate growth, fish record water temperatures in their body tissues, such as their teeth and scales, over their lifespan of years to decades. These

tissues are an integrated record of mean annual temperature (MAT), probably the most useful measurement of terrestrial temperature. For this study, we evaluate the $\delta^{18}O$ values of phosphate-rich non-migrating material from gar fish as an emerging methodology in the pursuit of terrestrial climate history.

Vertebrate bone, tooth dentin, and enamel contain calcium phosphate, primarily in the form of hydroxyapatite $Ca_5(PO_4)_3(OH)$. Of the biogenic apatites, enamel is the densest, nearly inorganic, and highly crystalline, and thus is known to be the most resistant to isotopic resetting during fossilization (Ayliffe et al., 1994; Koch et al., 1997). Phosphate is more resistant to isotopic resetting than carbonate (e.g., Grimes et al., 2003) and is therefore more ideal for paleoclimate studies.

The isotopic composition of oxygen in biogenic phosphate ($\delta^{18}O_p$) and carbonate ($\delta^{18}O_c$) are in equilibrium with body fluid during growth (e.g., Iacumin et al., 1996). The body water in turn is directly related to the isotopic composition of ingested water ($\delta^{18}O_w$), either from food, drinking water, or water vapor uptake (Luz et al., 1984). The $\delta^{18}O_c$ in modern fish apparently does not relate to either the isotopic composition or the temperature of the water in which the fish lived (Iacumin et al., 1996; Kolodny and Luz, 1991). Where $\delta^{18}O_c$ falls short in fish and other marine multicellular organisms, the more robust $\delta^{18}O_p$ demonstrates a clear temperature-dependent fractionation between biogenic phosphate oxygen and water. Since the oxygen isotopic exchange among inorganic dissolved phosphate and water is depleted in ^{18}O compared to the fractionation in biogenic phosphates, inorganic calibrations cannot be applied to biological systems (Lécuyer et al., 1999). A single phosphate oxygen equation was originally empirically developed for marine ectotherms, demonstrating that the $\delta^{18}O_p$ of bivalves and marine fish

closely follow the organism's water source (e.g. Kolodny et al., 1983; Longinelli and Nuti, 1973a, b).

Several following studies better defined the fractionation factor between $\delta^{18}O_p$, $\delta^{18}O_w$, and temperature, culminating in the discovery of a universal fractionation equation between dissolved phosphate and water related to a fundamental biosynthetic pathway using the enzyme inorganic pyrophosphatase (PPase) present in all organisms (Chang and Blake, 2015). PPase hydrolyzes inorganic pyrophosphate to inorganic phosphate, imparting a distinct fractionation between water and dissolved inorganic phosphate (DIP).

Interestingly, the fractionation factor (α) between body water, bone, or mineral phosphate in mammals does not follow this pattern and seems to vary according to species (e.g. Ayliffe and Chivas, 1990; Longinelli, 1984; Luz et al., 1990). The further fractionation in mammals indicates that taxon-specific fractionation equations may be necessary for certain species, which cannot be explained by the universal fractionation factor alone. The final phosphate oxygen isotopic composition of hard tissues is the result of the mineralization temperature, the initial oxygen isotopic composition of the dissolved phosphate in body fluids, and the biosynthetic pathway using PPase, and further 'vital effects' if the hard tissue is found in mammals.

Accounting for the taxon-specific relationships of some organisms, we provide a new calibration using the ganoine scales found in Lepisosteidae, or gars. Gars are more primitive than the Teleosts used in previous empirical calibrations (Kolodny et al., 1983; Longinelli and Nuti, 1973a; Pucéat et al., 2010) and their enamel production is more similar to that of mammals than Teleosts due to underlying genetic factors (Braasch et al., 2016). As a freshwater ectotherm, gar bioapatite records a mineralization temperature as well as the $\delta^{18}O_w$ of the environment. Gars are

model species because of their widespread occurrence in lacustrine settings in the past and present.

Gars are an ancient ray-fined fish lineage which date back to at the Late Cretaceous at least 100 million years ago (Wright et al., 2012). Fossil gars have been found in Europe, India, South America, and north and central Africa in addition to North America. Modern gars retain a large geographic range, extending throughout North America and into Central America and the Caribbean (Grande, 2010). They are unique in that their ganoid scales are highly mineralized with hydroxyapatite and are not underlain with dentin. The enamel directly overlies bone. Ganoid scales are extremely resistant to degradation, and are abundant in the fossil record.

Pucéat et al. (2010) recalibrates the marine fish equation of Kolodny et al. (1983) and Longinelli and Nuti (1973a) using revised analytical methods. Improved methodology to measure $\delta^{18}O_p$ has resulted in the cheaper, safer, and more efficient analysis of its isotopic composition (O'Neil et al., 1994). O'Neil et al. (1994) chemically converts biogenic PO_4^{3-} to Ag_3PO_4 and combusts it with graphite to produce CO_2 that is then measured for $\delta^{18}O$. The equation of Pucéat et al. (2010) is the most widely used calibration using the Ag_3PO_4 method at present for phosphate minerals (e.g., Finnegan et al., 2011; Joachimski et al., 2012).

For this work, we collect modern gar scales from a wide latitudinal range of lakes and rivers in the United States and calibrate their temperature-$\delta^{18}O_p$-$\delta^{18}O_w$ relationship with the revised Ag_3PO_4 method. Environmental influences on $\delta^{18}O_p$ are evaluated and its usefulness is assessed in reconstructing arguably non-diagenetic, regional $\delta^{18}O_w$ and temperature signals.

2. Materials and Methods

2.1. Model Organism, Specimen Acquisition and Site Location

Wild specimens of longnose gar (*Lepisosteus osseus*) and shortnose gar (*Lepisosteus platostomus*) scales were collected over the summer and late fall of 2014 under Yale University Institutional Animal Care and Use Committee Protocol #2012-10681 (Table S1 and Figure 1). Specimens were acquired either personally or with the assistance of the Mississippi Wildlife, Fisheries, & Parks Department, the Illinois Department of Natural Resources, and the Tennessee Wildlife Resources Agency through a combination rod and reel, gill netting, and electrofishing. Further gar specimens were loaned from the Yale Peabody Museum (YPM), Florida Museum of Natural History (UF), Texas Natural Science Center (TNSC), and the Chicago Field Museum (FMNH).

Wild caught fish were used in lieu of those reared from fry in tanks largely because of the extensive amount of time needed to raise these fish into adulthood, as their growth rates only begin to slow at four years of age, or roughly the beginning of sexual maturity (Netsch and Witt, 1962). An extensive, closely monitored tank set-up and feeding regimen is also needed to promote growth (Solomon, 2012). Working with museum collections as well as with state parks and wildlife departments to collect live fish was the most cost and time effective.

Because gars from the *Lepisosteus* and *Atractosteus* genera are able to hybridize (Herrington et al., 2008), any gars from these genera could potentially be used. For the sake of consistency, the paleothermometer is restricted to a single genus. When *Lepisosteus osseus* is not readily available, a sister taxon, *Lepisosteus platostomus*, the shortnose gar, is used.

Lepisosteus osseus, or the longnose gar, is the most widely spread extant gar species in North America. Its range spreads from the tributaries feeding the Mississippi River to the Atlantic coastline. Although the longnose gar has not yet been radio tagged and tracked, the tagging of a closely related sister species, *Atractosteus spatula*, the alligator gar, showed that it does not move more than 12.25 km (Sakaris et al., 2003). The restricted home range of any single individual, tolerance to salinities up to 31 ppt and temperatures from 4° to 31°C (McGrath, 2010), and easy accessibility make it an ideal model species as each specimen can be assigned a specific temperature and $\delta^{18}O_w$ composition.

2.2. Silver Phosphate Precipitation

For live fish that were caught as well as museum specimens, a 1 to 2 cm^2 section of scales were cut from the left side of the fish behind the pectoral fin. The right side was left intact for archival purposes. The scales were exposed to dermestid beetles for several weeks to remove overlying tissues.

From the cut section, 0.07 grams of scales were removed and placed in 30% H_2O_2 for a month to remove residual organic matter. Using the methodology of Vennemann et al. (2002) to further remove organics, samples were soaked in 2.5% NaOCl for 24 hours followed by 0.1 M NaOH for 48 hours before dissolution in 2M HNO_3.

Following methods of Liang (2005) and Liang and Blake (2006), modified from Kolodny et al. (1983), dissolved scales were first precipitated as ammonium phosphomolybdate (APM). The APM crystals were dissolved, filtered, and then dissolved phosphate was re-precipitated as magnesium ammonium phosphate (MAP). MAP crystals were dissolved in nitric acid and

cations removed with a resin before trisilver phosphate (Ag_3PO_4) was precipitated. Ag_3PO_4 was vacuum roasted at 550°C to remove residual organics and water.

Oxygen isotope analyses were performed at the YIBS Earth System Center for Stable Isotope Studies (ESCSIS) at Yale University using a Thermo-Chemolysis Elemental Analyzer (TC/EA) coupled to a Delta+ XP continuous flow isotope ratio monitoring mass spectrometer (Thermo-Finnigan, Germany) with a precision of ±0.3‰ (1 SD). Ag_3PO_4 crystals were heated to 1450°C in a graphite reactor to release O_2 which reacts with graphite to produce CO. The resultant CO was entrained in a He carrier gas, passed through a gas chromatograph (GC) and introduced into the mass spectrometer. $\delta^{18}O_{phosphate}$ values were calibrated against conventional fluorination standards according to Vennemann et al. (2002). All oxygen isotope data are reported as $\delta^{18}O$ in per mil relative to the VSMOW international reference standard. $\delta^{18}O_p$ values are standardized to two internal lab standards, YR1-a and YR3-2, with values of -5.49‰ and 33.64‰, respectively, for each run.

Water samples from each locality were analyzed on the same Delta+ XP with a GasBench (Thermo-Finnigan, Germany). Yearly $\delta^{18}O_w$ values of rivers using the coordinates of each specimen were taken from the Global Network of Isotopes in Rivers (GNIR) database hosted by the International Atomic Energy Agency (IAEA/WMO, 2018). Yearly temperatures were averaged for 15 years before the collection date of the gar specimen (National Centers for Environmental Information, 2022). Temperatures were converted to river temperature using the relationship $T_{atmosphere} = 1.01*t_{river} - 1.13$; river temperatures are approximately 1°C higher than ambient temperature (Fricke and Wing, 2004).

3. Results

Oxygen isotope compositions ($\delta^{18}O_p$) of gar scales vary from 15.71‰ to 18.76‰ (SE= 0.084, n = 51, Table 1). Standard error is calculated from the analytical error for each $\delta^{18}O_p$ measurement with replicate uncertainty. All errors are at 1σ.

Oxygen isotopes in phosphate are dependent on two variables, temperature (T), and the oxygen isotopic composition of water ($\delta^{18}O_w$). Of these, the error on $\delta^{18}O_w$ (SE = 0.320) is larger than that on T (SE = 0.185). Uncertainty for T is $\sqrt{n}$. For the sake of brevity, $\delta^{18}O_w$–$\delta^{18}O_p$ is shortened to Δ_{P-W}, notation first used in Kolodny et al. (1983) and elucidated in Slater et al. (2001). Following notation used in previous calibrations, T is graphed against Δ_{P-W} and a linear regression model is applied to the data (Figure 2) (Zaarur et al., 2013, supplementary information). Δ_{P-W} contains the largest error ($\delta^{18}O_w$) so it is placed on the dependent (Y) axis while T, with the smaller error, is placed on the independent (X) axis. All statistical analyses are done with T as the independent variable. The reduced X^2 = 1.031 indicates that the best-fit linear regression adequately captures the variance in the dataset.

The Δ_{P-W} residuals have a marginally larger standard deviation (σ = 0.534) than the standard deviation of the replicates, or multiple fish specimens, from each of ten sites (n = 39, df = 29, σ = 0.532). Both of these are smaller than the standard deviation of Δ_{P-W} (σ = 1.133) and T (σ = 2.663), indicating that a large source of noise in the dataset is natural variation.

Higher latitude sites undergo a wider temperature fluctuation than lower latitude sites. The lowest latitude site, Coldspring, TX has a yearly standard temperature deviation of 6.81°C with a range between 9.86°C in January and 28.07°C in August. The highest latitude site, Gull Lake, MI ranges from -5.88°C in January to 22.69°C in July with a standard temperature

198 deviation of 10.34°C. This imparts a wider temperature error at the colder endpoint of the
199 temperature-$\delta^{18}O_w$-$\delta^{18}O_p$ relationship.

200 The distribution of the data is tighter for samples from closed basins (e.g., Tims Ford
201 Lake, TN) and more dispersed for samples from large drainages (e.g., Rice Lake, off Illinois
202 River, IL.). Large variations in $\delta^{18}O_w$ coincide with large variations in $\delta^{18}O_p$. The $\delta^{18}O_w$ of river
203 water is a combination of precipitation and groundwater values. At coastal sites, such as those
204 from Mississippi and Florida, the precipitation contribution is higher than that found in some
205 inland sites, such as Illinois. The isotopic signature of storm tracks from the Gulf of Mexico
206 imparts a higher $\delta^{18}O_w$ variation at these sites.

207 Gars are known to experience faster growth during the late spring before spawning (e.g.
208 Love, 2003; Netsch and Witt, 1962), so comparisons were made to May through August
209 averages in addition to yearly temperatures. $\delta^{18}O_w$ were the averages from the same months.

210

211 **4. Discussion**

212 *4.1 New Paleothermometer for Gar Scales*

213 This study shows that the oxygen isotopic composition of gar scales is correlated to both
214 the temperature and the oxygen isotopic composition of the source water (Figure 2, Table 1).
215 The inverse-regression method was used to calculate the calibration and confidence intervals.
216 Reliability ratios, λ (Carroll et al., 2006), indicate both variables are relatively insensitive to error
217 ($\lambda_{\Delta P-W} = 0.935$ and $\lambda_T = 0.995$). In contrast to other T-$\delta^{18}O_w$-$\delta^{18}O_p$ calibrations, temperature is
218 chosen as the independent variable on the horizontal axis as it has marginally less error than
219 Δ_{P-W}. Standard error (SE) is corrected for small sample size using Student's t distribution.

There is a marked difference between the recent marine bioapatite thermometry calibration, $T(°C) = 124.6 – 4.52(\delta^{18}O_p - \delta^{18}O_w)$ (Pucéat et al., 2010) and the two equations derived here (Figure 3). Reduced $X^2 = 1.031$ indicates the standard errors are within what is expected from this calibration. $SE(\Delta_{P–W})$ is reduced by sampling multiple fish specimen across multiple sites. 39 of the 51 samples were from 10 sites (n_s) with 3 or more different specimens (n_r), which directly affected the calculated confidence interval curves. Adequately minimizing error can be done by sampling at least $n_s = n_r = 4$ (Figure S2).

The calculated calibration for gar scales and mean annual river temperatures (MAWT) is (Figure 3):

$$T(°C) = -2.072(\Delta_{P–W}) + 61.973 \ (R^2 = 0.778), \quad (1)$$

and that for mean-summer river temperatures (MSWT) is:

$$T(°C) = -1.152(\delta^{18}O_{phosphate} - \delta^{18}O_{water}) + 50.081 \ (R^2 = 0.6503) \quad (2)$$

where T is in °C and $\Delta_{P–W}$ is in SMOW.

These equations differ in both intercept and slope as well as degree of linear fit, which we attribute to indeterminate gar scale growth recording a MAWT signal (Figure 3). Both calibrations (1, 2) have a shallower slope when using gar scales as compared to the Pucéat et al. (2010) calibration using fish teeth. All teleosts and marine invertebrates were previously assumed to follow the same temperature-$\delta^{18}O_w$-$\delta^{18}O_p$ equation (Kolodny et al., 1983; Longinelli

and Nuti, 1973a, b; Pucéat et al., 2010). This may not be the case for the freshwater gar fish, and for Holostei as a whole. Applying the Pucéat et al. (2010) whole fish-tooth calibration to gar scales returns artificially warmer MAWT temperatures of 2 to 11°C (Figure 3), corresponding to a 0.5 to 2.5‰ difference in $\delta^{18}O_p$.

Summer sampled water oxygen isotope values are in agreement with summer $\delta^{18}O_w$ recorded by Kendall and Coplen (2001)(Figure S2, Table S2) and support using their annual $\delta^{18}O_w$ measurements.

4.2. Environmental influences on recorded $\delta^{18}O_{phosphate}$

The MAWT calibration has a significantly better fit than the MSRT calibration as it accounts for a larger fraction of the MAWT and $\delta^{18}O_{phosphate}$ variation. Error, at least in MAWT, is reduced through time averaging. For the sites chosen, daily and monthly ambient temperatures fluctuate widely while yearly temperatures are relatively consistent. Many of these sample localities experience more sunny days and thus higher evaporation in the summer months while other sample localities receive their greatest precipitation in the spring and early summer. Like temperature, precipitation can still vary widely on a monthly basis. These changes in evaporation and precipitation affect $\delta^{18}O_w$ and change the recorded $\delta^{18}O_p$.

Marine systems, particularly in large open oceanic basins, have less variation in both temperature and oxygen isotopic values than their terrestrial equivalents (e.g., Bowen and Revenaugh, 2003; LeGrande and Schmidt, 2006). $\delta^{18}O_w$ in the ocean is closely correlated with evaporation and precipitation, as manifested in salinity. From the tropics to mid-latitudes oceanic $\delta^{18}O_w$ ranges from ~-6 to ~+2 ‰ (LeGrande and Schmidt, 2006). On land from the equator to the

Arctic Circle, $\delta^{18}O_w$ ranges from ~-20 to ~0 ‰ (IAEA/WMO, 2018). Monthly high and low mean temperatures of the same latitudinal range on land varies from ~-30 °C to ~+40 °C whereas those from the ocean from ~0 °C to ~+28 °C (National Centers for Environmental Information, 2022).

Large oceanic basins are unaffected by most of the processes that lead to the wide range of $\delta^{18}O_w$ and temperatures experienced by lacustrine systems. Lake size, amount of mixing, residence time, catchment size, and whether the body of water is open or closed are some of the many factors that affect lacustrine $\delta^{18}O_w$ (Leng and Marshall, 2004). To illustrate, larger lakes are generally better mixed than their smaller counterparts, so daily, monthly, and seasonal fluctuations in precipitation $\delta^{18}O_w$ is averaged. Closed lakes, particularly those in arid climates, have heavier $\delta^{18}O_w$ values as they are more affected by evaporation, .

The larger variation in freshwater lakes compared to marine basins is alluded to in Kolodny et al. (1983). The upper 200 m in Lake Baikal in Siberia, Russia is highly stratified by temperature, ranging from 2 to 12 °C. Below the thermocline, temperatures are relatively constant at 3.2 to 4 °C. Kolodny et al. (1983) accounts for temperature differences by only sampling fish who live in a narrow depth range. $\delta^{18}O_w$ is relatively consistent at all depths at -15.9 ± 0.2‰ (Seal II and Shanks III, 1998). As the deepest and largest freshwater lake by volume, water turnover time is slow, taking over ~300 years. Evaporation in this lake contributes from 13 to 19% of its total water loss and the remainder is through riverine outflow (Seal II and Shanks III, 1998 and references therein). The isotopic composition of riverine and precipitation influx of -15.2‰ for $\delta^{18}O_w$ reinforces the long residence time of the water, as Lake Baikal has

not reached a steady state where the lake $\delta^{18}O_w$ is heavier than the influx $\delta^{18}O_w$ as would be expected from large amounts of evaporation.

In comparison, the main water source to Lake Kinnereth (Sea of Galilee) in Israel is the Jordan River, not precipitation. The mean annual $\delta^{18}O_{precipitation}$ for Safed, Israel is -6.22 ± 0.69‰ (IAEA/WMO, 2018) and a stable -7.51‰ $\delta^{18}O_w$ for the nearby Dan tributary to the Jordan River (Gat and Dansgaard, 1972). Lake Kinnereth itself ranges from -2.5 to +0.5‰ $\delta^{18}O_w$ (Gat, 1984), indicative of heavy evaporation. Kolodny et al. (1983) measure $\delta^{18}O_p$ of three fish species from this lake, but use a $\delta^{18}O_w$ of -2.1‰ which is on the lighter side. Zaarur et al. (2016) measure +0.5‰ for the southern shoreline of the lake during the summer months. By adjusting the Lake Kinnereth samples of Kolodny et al. (1983) to the average $\delta^{18}O_w$ composition of -1‰ and accounting for the error on $\delta^{18}O_w$, these fish plot in between the MAWT calibration for gar scales and the Pucéat et al. (2010) calibration for marine fish (Figure 3).

The same error that occurs with high evaporation is seen in the seasonally heavy $\delta^{18}O_w$ measured from localities in Texas, USA (Figure S2). One gar (TNSC 15583) from Hempstead, TX was culled from the final dataset because of the large seasonal variation in $\delta^{18}O_w$ and the large error on $\delta^{18}O_p$ (21.89‰ ± 1.10), possibly due to incomplete mineralization as the specimen had not yet reached adulthood. Incomplete mineralization can result in a $\delta^{18}O_p$ signal that reflects the oxygen isotopic composition of phosphate species other than the phosphate from bioapatite, such as dissolved inorganic phosphate.

Large mixed bodies of water are more robust record holders, such as Lake Baikal or Tims Ford Reservoir, TN, USA (this study) than highly evaporative ones such as Lake Kinnereth or many streams and rivers in Texas where evaporation exceeds precipitation. The isotopic

composition of source waters, either from upstream riverine input or precipitation, can also affect the $\delta^{18}O_w$ and therefore the $\delta^{18}O_p$ recorded by the fish, either freshwater or marine. For paleoclimate studies, fish scales and teeth should only be sampled from areas where $\delta^{18}O_w$ can be well constrained or where temperature can be estimated independently.

4.3. Potential seasonal bias in scale growth

Nuances in growth patterns are recorded in scales. Scales begin mineralizing within the first year and are retained throughout life (Thomson and McCune, 1984) so their isotopic signal is time averaged over the lifetime of the fish. Growth artifacts appear as banding in the underlying bone and ridges in the overlying ganoine (Figure 5). Five to six of these bands are formed within the first two years of life, and formation rates decrease as the fish ages to eventually only one or two a year (Thomson and McCune, 1984). The oldest, largest gars often do not lay down even one band a year. Additionally, band count against standard length in gars gives a straight line. This suggests that instead of correlating to incremental growth, with periods of quiescence, the bands better correlate to increasing scale size so as to maintain the constant standard length growth seen throughout the gar's life (Love, 2003; Netsch and Witt, 1962). The data from this study are considered climatic averages experienced by the fish during life since they are from ground whole scales.

Temperature extremes may adversely impact growth in fry (Solomon, 2012) as they are the most vulnerable at this age with high mortality rates (Haase, 1969). Regardless, gars are capable of thriving in a wide temperature range, from Lake Champlain in Vermont for the Longnose Gar to the Yucatán Peninsula in Mexico for the Tropical Gar. Coupled with

329 uninterrupted growth rates, temperature extremes only result in torpor, not complete cessation of
330 movement and growth in adults. The spotted gar is the most physically active from March until
331 early June, coincident with preparation before spawning (Snedden et al., 1999). Alligator gar
332 also display the same behavior of increased movement during pre-spawn periods (Buckmeier et
333 al., 2013).

334 Of note is that females grow at faster rates than males, live longer, and are larger,
335 although they reach sexual maturity later in life (Netsch and Witt, 1962). We did not account for
336 the sex of our gar specimens given that it is difficult to distinguish from external features and sex
337 was assumed to not affect isotopic composition. Gars are in the best condition preceding
338 spawning events with their highest gonadosomatic indices (GSI) (Johnson and Noltie, 1997;
339 Love, 2003). Both male and, even more so, female gar lose a significant amount of body mass
340 after spawning (Johnson and Noltie, 1997), which reduces growth rate. Spawning only occurs
341 after a temperature threshold is reached; this timing may change from year to year but is always
342 in the late spring, from late April to June (Echelle and Riggs, 1972; Haase, 1969; Johnson and
343 Noltie, 1997; Netsch and Witt, 1962).

344 Growth studies in gars, like most fish, have centered on using either branchiostegal rays
345 (Haase, 1969; Johnson and Noltie, 1997; Klaassen and Morgan, 1974; Netsch and Witt, 1962) or
346 otoliths to better infer age (Ferrara, 2001; Smylie et al., 2016). Distinct banding is present in both
347 structures, and each region between annuli are considered to be equivalent to a year of growth.
348 Generally in the otoliths of fish, opaque and translucent bands alternate and are seasonally
349 related, with opaque bands indicating faster growth and translucent zones forming during periods
350 of slower growth, although conflicting conclusions about timing indicate that otolith formation is

351 also species and latitude (e.g. tropical, temperate, or subpolar) dependent (Beckman and Wilson,
352 1995). Longnose gars emplace opaque edges anywhere from February to May (Smylie et al.,
353 2016) and alligator gars in May (Buckmeier et al., 2012) coincident with increase in mass and
354 activity levels in preparation for spawning.

355 All of the locations in this study appear to have spring temperatures, more specifically the
356 dates associated with the spawning of gars and their highest activity, that are within error to
357 MAT and therefore MAWT. For example, in Benton, IL, the NOAA reference location for the
358 Rend Lake Dam samples recorded MAT from 2000 until 2013 of 13.77 ± 0.74 °C. During the
359 same yearly interval, the average spring temperature, from March, April, and May, was 14.05 ±
360 1.47 °C. For Grenada, MS, from 2000 to 2013, the MAT was 16.82 ± 0.62 °C and the March,
361 April, and May average from the same time interval was 16.91 ± 1.25 °C.

362 If there is a growth bias in scales towards the spring as seen in otoliths and branchiostegal
363 rays, it can be assumed that it is equivalent to MAWT. However, the enamel of scales only
364 superficially corresponds to age and it loses its efficacy as an age estimator with time (Thomson
365 and McCune, 1984). In older gars, because age estimates from scales are underestimates
366 (Buckmeier et al., 2012), it is unlikely that gar scale formation can be completely explained by
367 spring seasonal formation as displayed in otoliths and branchiostegal rays. The better correlation
368 between $\delta^{18}O_p$ and MAWT instead of MSWT confirms this.

369

370 *4.4. Genetic basis for unique calibration*

371 Two separate fractionations occur between water and dissolved inorganic phosphate
372 (DIP) and between DIP and biological tissues, including DNA, mineral bioapatite, and

biomolecules and soft tissues (Blake et al., 2005; Blake et al., 2016; Chang and Blake, 2015). The distinct fractionation between DIP and body water is caused by the intracellular enzyme reaction involving inorganic pyrophosphatase (PPase). The amino acid sequence of PPase of prokaryotes (bacteria and archaea) and eukaryotes (fungi, plants, and animals) differs substantially but the active site in the resultant enzyme is remarkably conserved across domains (e.g. Cooperman et al., 1992). The fractionation between DIP and water using PPase hence is likely ubiquitous (Chang and Blake, 2015).

The slopes of the DIP−water oxygen isotope fractionation using the marine teleost data of Pucéat et al. (2010) and yeast data of Chang and Blake (2015) are identical within error. This reaction is the primary process that links the $\delta^{18}O$ composition of dissolved phosphate within cells and body water to environmental factors such as temperature and river isotopic composition (Blake et al., 2016; Chang and Blake, 2015).

Even though there is no apparent further fractionation in tooth formation in teleosts from DIP to bioapatite, as the $\delta^{18}O_p$ values are nearly identical to those predicted from the $\delta^{18}O_w$–$\delta^{18}O_p$ fractionation alone, DIP in the body water of an organism and cytoplasm of microbial cells may be further fractionated during the creation of phosphatic biomass. There is evidence that this second fractionation may be species-dependent, due to a combination of natural history, habitat such as humidity and aridity for terrestrial species, and genetic factors. Terrestrial, species-specific phosphate-oxygen isotope calibrations have been calculated for numerous endotherms: rabbits (Huertas et al., 1995), mice, cattle, sheep (D'Angela and Longinelli, 1990), kangaroos (Ayliffe and Chivas, 1990), humans (Daux et al., 2008; Longinelli, 1984) and pigs (Longinelli, 1984). These calibrations all follow the same linear trend with positive slopes. Differences arise

395 if the species is water dependent or drought tolerant (Kohn and Cerling, 2002), as environmental
396 relative humidity has a strong influence on these calibrations (Ayliffe and Chivas, 1990).
397 Since humidity should be irrelevant for an aquatic species, feeding patterns could
398 partially explain the difference in slope seen in the gar calibration presented here when compared
399 to previously-observed calibrations using both marine and mammalian species. For example,
400 African ungulates eat a wide range of food with unique $\delta^{18}O$ and, coupled with varying
401 physiologies (Kohn et al., 1996), have unique $\delta^{18}O_p$-$\delta^{18}O_w$ trends. In humans, since vegetables
402 and some meats consist of a large weight percent of water, an offset of 0.6‰ to 0.7‰ per mil can
403 be attributed to diet alone (Daux et al., 2008). Because gars are opportunistic feeders but mainly
404 feed on smaller fish, with only the occasional insect or crustacean (Goodyear, 1967), we assume
405 that diet has a minimal influence on $\delta^{18}O_p$ for gar scales as all of these animals experience the
406 same $\delta^{18}O_w$.
407 Oxygen in the phosphate of mammals comes from air in addition to food and drinking
408 water, and the relative portions of these sources ultimately affect recorded $\delta^{18}O_p$. If there is
409 complete exchange of all four oxygens in PO_4^{3-} with water via PPase catalysis, the slope of the
410 $\delta^{18}O_p$-$\delta^{18}O_w$ trend will be 1 (Blake et al., 2005). A slope less than 1 indicates incomplete oxygen
411 transfer from body water to PO_4^{3-}, and a slope greater than 1 can indicate influence from
412 metabolic water or a large dietary or inhaled air effect, either moisture via humidity or the
413 isotopic signature of O_2 itself. The slopes of $\delta^{18}O_p$-$\delta^{18}O_w$ for mammals range from 0.49 to 0.57
414 for rats (Luz et al., 1984; Navarro et al., 2004), 1.01 for cattle (D'Angela and Longinelli, 1990),
415 1.34 for foxes (Iacumin and Longinelli, 2002), and 1.54 for humans (Daux et al., 2008; Levinson

et al., 1987; Longinelli, 1984; Luz et al., 1984). In gars, when temperature is held constant, the slope is 1 (Figure S2), confirming that $\delta^{18}O_w$ is the main source of oxygen.

Most notably, there are differences in biomineralization at the genetic level between the taxonomic group that includes gar fish and that of teleosts. Primitive gars are genetically more similar to mammals as they produce true enamel while more derived teleosts produce enameloid (Braasch et al., 2016). Gars, like mammals, have distinct proteins and enzymes that may cause differences in kinetic fractionation when oxygen in DIP is incorporated into the mineral lattice of biogenic apatite.

Mammalian enamel is produced by several proteins: enamelins, amelogenins, ameloblastins, tuftelins and proteinases (Fincham et al., 1999). Teleostei only employs enamelins, producing enameloid. Both enamel and enameloid are highly mineralized ectodermal tissues but they differ in that enamel consists of monolayers with incremental lines and structured prisms while enameloid consists of crystal bundles and is aprismatic (Fincham et al., 1999; Richter and Smith, 1995). More importantly, in enameloid development, odontoblasts create a collagen-rich organic matrix which is dissolved by dental epithelial cells. These dental epithelial cells promote final crystal growth through inorganic ion supply (Sasagawa et al., 2009).

Enamel has a distinct precursor mineral not found in enameloids, octacalcium phosphate ($Ca_8H_2(PO_4)_6 \cdot 5H_2O$), which can hydrolyze to hydroxyapatite ($Ca_5(PO_4)_3OH$), and serves as a template for hydroxyapatite precipitation. Furthermore, amelogenin is important in maintaining the crystal spacing of newly precipitated hydroxyapatite. Enameloid crystals are only shaped by

dentin collagen and dentin phosphoprotein. Enamel crystals utilize these in combination with amelogenin (Simmer and Fincham, 1996) which is absent in enameloid production.

The teeth and scales of both *Lepisosteus sp.* and *Polypterus sp.* produce enamel and enameloid (Sasagawa et al., 2009). During scale formation, the preganoine matrix is collagen-free (Sire et al, 1994). The final ganoine thus lacks the collagen fibers of enameloid and is preceded by dentin deposition, making it a true enamel (Sire et al., 1987). Immunohistochemical studies have determined that the amelogenin protein that forms ganoine and teeth in gars is homologous with the mammalian amelogenin protein because it possesses domains that are shared with those found in mammals (Ishiyama et al., 1999; Sasagawa et al., 2014). Preganoine was found to contain the amelogenin protein, the presumable agent for the oxygen isotope fractionation between body water and the phosphate found in the bioapatite of higher vertebrates.

The enamel link between gars and mammals was further supported with the sequencing of the *L. oculatus* genome (Braasch et al., 2016). Teleosts, mammals, and gars all have different genetic modifications of secretory calcium-binding phosphoproteins (Scpp). Interestingly, gars have orthologs of SCPP genes found only in teleosts and different SCPP genes found only in lobe-finned vertebrates so essentially gars genetically straddle the two groups. Specifically, the gar *ambn* and *enam* genes have a genetic homolog in lobe-finned vertebrates; similar but not identical sequences are identified in Teleosts. None of the SCPP genes that teleosts use to mineralize enameloid directly corresponds to tetrapod SCPPs (Kawasaki et al., 2005). The genetic instructions that gars use to create ganoine are more similar to those that mammals and reptiles use to produce enamel than the ones that teleosts use for enameloid.

458 Teleosts have much faster evolutionary rates than do gars and their allies, and it appears
459 as though they lost the true enamel protein genes along their evolutionary path (Braasch et al.,
460 2016), likely after their total genome duplication event. The archaic structure of cap enameloid
461 and collar enamel is retained in *Polypterus* and *Lepisosteus* (Sasagawa et al., 2013) and their
462 biomineralization pathway similarity to the mammalian one implies that their temperature-$\delta^{18}O_w$-
463 $\delta^{18}O_p$ relationship is more similar to that found in mammals than to marine fish and invertebrates.
464 Further study is needed to determine any kinetic isotopic effects associated with the enamelin or
465 amelogenin proteins during enamel formation.
466 The observation that gar scales show banding is similar to the growth striations present in
467 mammalian teeth, termed the striae of Retzius. These striations are mandated by amelogenesis
468 and ultimately circadian rhythms. Growth intervals can range from days to weeks to years
469 (Boyde, 1964; Bromage, 1991; Dean, 1987). Because the frequency of ridges in scales decrease
470 as gars age, striations are presumably more a growth artifact than discrete intervals of growth
471 such as otoliths or tree rings.
472
473 **5. Conclusions**
474 Gar scales have a relationship between MAWT, $\delta^{18}O_p$, and $\delta^{18}O_w$ that is significantly
475 different from the one for marine fish postulated by Pucéat et al. (2010). Genomics indicates that
476 ganoine formation in gars is more closely matches that of mammals than that of teleosts (Braasch
477 et al., 2016) as both gars and mammals use enamelin and amelogenin proteins. Terrestrial
478 mammals have species-specific $\delta^{18}O_p$-$\delta^{18}O_w$ relationships and gars appear to have a species-
479 specific calibration as well.

Scales do not form in the same manner as otoliths or branchiostegal rays as the frequency of growth bands decreases with age. While not expected, any bias in recorded temperatures in scales would reflect spring temperatures preceding spawning events when gars are the most active. Riverine spring temperatures at all of the localities are within error to MAWT.

Gars that swim in large bodies of water with little evaporation instead of in smaller bodies of water with large precipitation or river influxes record relatively invariable $\delta^{18}O_p$ because of more constrained $\delta^{18}O_w$. For paleoclimate studies, the best gar scales are those from environments that fit these criteria. Gar scales have tentatively been used in paleoclimate research (Fricke et al., 1998; Fricke and Pearson, 2008) and with this new fractionation equation, their future in unraveling the past is very promising. By applying the temperature-$\delta^{18}O_w$-$\delta^{18}O_p$ relationship found in modern gar scales to fossil gar scales, terrestrial climate can be elucidated. If the temperature variable is constrained by other means, then the $\delta^{18}O_w$ value can be calculated, thus providing information about the hydrological cycle.

Acknowledgements

This work was supported by a grant from the U.S. National Science Foundation (NSF-OCE-0928247 and NSF-OCE-1129499) as NASA (N00199-1073649) awarded to R. E. Blake. A grant from the Yale Institute of Biospheric Studies awarded to K.E. Gray helped fund fieldwork. Sincere thanks go to Mark Pagani for his guidance and advice on the overall theme of this project. Hui Li and Sae Jung Chang assisted with Ag_3PO_4 precipitation. Brad Erkkila, Jonas Karosas, and Marvin Wint of the Yale Analytical and Stable Isotope Center helped with TC/EA troubleshooting and analyses. Greg Watkins-Colwell of the Yale Peabody Museum assisted in

gar scale removal and cleaning. Rob Hilsabeck, Jana Hirst, and John Wisher of Illinois Department of Natural Resources as well as Nathan Singer of the Tennessee Wildlife Resources Agency helped to acquire modern Lepisosteids. Adam E. Cohen at the University of Texas at Austin Texas Natural History Collections, Caleb McMahan at the Chicago Field Museum, Matt Roberts at the Mississippi Museum of Nature and Science and Robert H. Robins at the Florida Museum of Natural History all took the time to prepare gar scales from their collections that were used in this study.

References

Ayliffe, L.K., Chivas, A.R., 1990. Oxygen isotope composition of bone phosphate of Australian kangaroos: Potential as a paleoenvironmental recorder. Geochimica et Cosmochimica Acta 54, 2603-2609.

Ayliffe, L.K., Chivas, A.R., Leakey, M.G., 1994. The retention of primary oxygen isotope compositions of fossil elephant skeletal phosphate. Geochimica et Cosmochimica Acta 58, 5291-5298.

Beckman, D.W., Wilson, C.A., 1995. Timing of fish otolith opaque zone formation, in: Secor, D.H., Dean, J.M., Campana, S.E. (Eds.), Recent developments in fish otolith research. University of South Carolina Press, Columbia, South Carolina.

Blake, R.E., O'Neil, J.R., Surkov, A.V., 2005. Biogeochemical cycling of phosphorus: Insights from oxygen isotope effects of phosphoenzymes. American Journal of Science 305, 596-620.

Blake, R.E., Surkov, A.V., Stout, L.M., Li, H., Chang, S.J., Jaisi, D.P., Colman, A.S., Liang, Y., 2016. DNA thermometry: a universal biothermometer in the $^{18}O/^{16}O$ ratios of PO_4 in DNA. American Journal of Science 316, 813-838.

Bowen, G.J., Revenaugh, J., 2003. Interpolating the isotopic composition of modern meteoric precipitation. Water Resources Research 39, 1299.

Boyde, A., 1964. The Structure and Development of Mammalian Enamel, Department of Anatomy. University of London, London.

Braasch, I., Gehrke, A.R., Smith, J.J., Kawasaki, K., Manousaki, T., Pasquier, J., Amores, A., Desvignes, T., Batzel, P., Catchen, J., Berlin, A.M., Campbell, M.S., Barrell, D., Martin, K.J., Mulley, J.F., Ravi, V., Lee, A.P., Nakamura, T., Chalopin, D., Fan, S., Wcisel, D., Cañestro, C., Sydes, J., Beaudry, F.E.G., Sun, Y., Hertel, J., Beam, M.J., Fasold, M., Ishiyama, M., Johnson, J., Kehr, S., Lara, M., Letaw, J.H., Litman, G.W., Litman, R.T., Mikami, M., Ota, T., Saha, N.R., Williams, L., Stadler, P.F., Wang, H., Taylor, J.S., Fontenot, Q., Ferrara, A., Searle, S.M.J., Aken, B., Yandell, M., Schneider, I., Yoder,

J.A., Volff, J.-N., Meyer, A., Amemiya, C.T., Venkatesh, B., Holland, P.W.H., Guiguen, Y., Bobe, J., Shubin, N.H., Di Palma, F., Alföldi, J., Lindblad-Toh, K., Postlethwait, J.H., 2016. The spotted gar genome illuminates vertebrate evolution and facilitates human-teleost comparisons. Nature Genetics 48, 427-437.

Bromage, T.G., 1991. Enamel incremental periodicity in the Pig-Tailed Macaque: A Polychrome Fluorescent Labeling Study of Dental Hard Tissues. American Journal of Physical Anthropology 86, 205-214.

Buckmeier, D.L., Smith, N.G., Daugherty, D.J., 2013. Alligator Gar Movement and Microhabitat Use in the Lower Trinity River, Texas. Transactions of the American Fisheries Society 142, 1025-1035.

Buckmeier, D.L., Smith, N.G., Reeves, K.S., 2012. Utility of Alligator Gar Age Estimates from Otoliths, Pectoral Fin Rays, and Scales. Transactions of the American Fisheries Society 141, 1510-1519.

Carroll, R.J., Ruppert, D., Stefankski, L.A., Crainiceanu, C.M., 2006. Measurement error in nonlinear models. CRC Press.

Chang, S.J., Blake, R.E., 2015. Precise calibration of equilibrium oxygen isotope fractionations between dissolved phosphate and water from 3 to 37°C. Geochimica et Cosmochimica Acta 150, 314-329.

Cooperman, B.S., Baykov, A.A., Lahti, R., 1992. Evolutionary conservation of the active site of soluble inorganic pyrophosphatase. Trends in Biochemical Sciences 17, 262-266.

D'Angela, D., Longinelli, A., 1990. Oxygen isotopes in living mammal's bone phosphate: Further results. Chemical Geology 86, 75-82.

Daux, V., Lecuyer, C., Héran, M.-A., Amiot, R., Simon, L., Fourel, F., Martineau, F., Lynnerup, N., Reychler, H., Escarguel, G., 2008. Oxygen isotope fractionation between human bone phosphate and water revisted. Journal of Human Evolution 55, 1138-1147.

Dean, M.C., 1987. Growth layers and incremental markings in hard tissues; a review of the literature and some preliminary observations about enamel structure in *Paranthropus boisei*. Journal of Human Evolution 16, 157-172.

Echelle, A.A., Riggs, C.D., 1972. Aspects of the Early Life History of Gars (Lepisosteus) in Lake Texoma. Transactions of the American Fisheries Society 101, 106-112.

Ferrara, A.M., 2001. Life history strategy of Lepisosteidae: Implications for the conservation and management of Alligator gar, Fisheries and Allied Aquacultures. Auburn University, Auburn, Alabama, p. 145.

Fincham, A.G., Moradian-Oldak, J., Simmer, J.P., 1999. The structural biology of the developing dental enamel matrix. Journal of Structural Biology 126, 270-299.

Finnegan, S., Bergmann, K., Eiler, J.M., Jones, D.S., Fike, D.A., Eisenman, I., Hughes, N.C., Tripati, A.K., Fischer, W.W., 2011. The magnitude and duration of Late-Ordovician-Early Silurian glaciation. Science 331, 903-906.

Fricke, H.C., Clyde, W.C., O'Neil, J.R., Gingerich, P., 1998. Evidence for rapid climate change in North America during the latest Paleocene thermal maximum: oxygen isotope compositions of biogenic phosphate from the Bighorn Basin (Wyoming). Earth and Planetary Science Letters 160, 193-208.

Fricke, H.C., Pearson, D.A., 2008. Stable isotope evidence for changes in dietary niche partitioning among hadrosaurian and ceratopsian dinosaurs of the Hell Creek Formation, North Dakota. Paleobiology 34, 534-552.
Fricke, H.C., Wing, S.L., 2004. Oxygen isotope and paleobotanical estimates of temperature and $\delta^{18}O$ latitude gradients over North American in Eocene. American Journal of Science 304, 612-635.
Gat, J.R., 1984. The stable isotope composition of Dead Sea waters. Earth and Planetary Science Letters 71, 361-376.
Gat, J.R., Dansgaard, W., 1972. Stable isotope survey of the fresh water occurrences in Israel and the northern Jordan rift valley. Journal of Hydrology 16, 177-212.
Goodyear, C.P., 1967. Feeding habits of three species of gars, Lepisosteus, along the Mississippi Gulf Coast. Transactions of the American Fisheries Society 96, 297-300.
Grande, L., 2010. An empirical synthetic pattern study of gars (Lepisosteiformes) and closely related species, based mostly on skeletal anatomy. The resurrection of Holostei. American Society of Ichthyologists and Herpetologists.
Grimes, S.T., Mattey, D.P., Hooker, J.J., Collinson, M.E., 2003. Paleogene paleoclimate reconstruction using oxygen isotopes from land and freshwater organisms: the use of multiple proxies. Geochimica et Cosmochimica Acta 67, 4033-4047.
Haase, B.L., 1969. An ecological life history of the longnose gar, Lepisosteus osseus (Linnaeus), in Lake Mendota and in several other lakes of southern Wisconsin, Zoology. University of Wisconsin, p. 225.
Herrington, S.J., Hettiger, K.N., Heist, E.J., Keeney, D.B., 2008. Hybridization between Longnose and Alligator Gars in Captivity, with Comments on Possible Gar Hybridization in Nature. Transactions of the American Fisheries Society 137, 158-164.
Huertas, A.D., Iacumin, P., Stenni, B., Chillón, B.S., Longinelli, A., 1995. Oxygen isotope variations of phosphate in mammalian bone and tooth enamel. Geochimica et Cosmochimica Acta 59, 4299-4305.
Iacumin, P., Bocherens, H., Mariotti, A., Longinelli, A., 1996. Oxygen isotope analyses of co-existing carbonate and phosphate in biogenic apatite: a way to monitor diagenetic alteration of bone phosphate? Earth and Planetary Science Letters 142, 1-6.
Iacumin, P., Longinelli, A., 2002. Relationship between $\delta^{18}O$ values for skeletal apatite from reindeer and foxes and yearly mean $\delta^{18}O$ values of environmental water. Earth and Planetary Science Letters 2002, 213-219.
IAEA/WMO, 2018. Global Network of Isotopes in Precipitation. The GNIP Database.
Ishiyama, M., Inage, T., Shimokawa, H., 1999. An immunocytochemical study of amelogenin proteins in the developing tooth enamel of the Gar-Pike, *Lepisosteus oculatus* (Holostei, Actinopterygii). Archives of histology and cytology 62, 191-197.
Joachimski, M.M., Breisig, S., Buggisch, W., Talent, J.A., Mawson, R., Gereke, M., Morrow, J.R., Day, J., Weddige, K., 2009. Devonian Climate and reef evolution: Insights from oxygen isotopes in apatite. Earth and Planetary Science Letters 284, 599-609.
Joachimski, M.M., Lai, X., Shen, S., Jiang, H., Luo, G., Chen, B., Chen, J., Sun, Y., 2012. Climate warming in the latest Permian and the Permian-Triassic mass extinction. Geology 40, 195-198.

Johnson, B.L., Noltie, D.B., 1997. Demography, growth, and reproductive allocation in stream-spawning Longnose gar. Transactions of the American Fisheries Society 126, 438-466.
Karhu, J.A., Epstein, S., 1986. The implication of the oxygen isotope records in coexisting cherts and phosphates. Geochimica et Cosmochimica Acta 50, 1745-1756.
Kawasaki, K., Suzuki, T., Weiss, K.N., 2005. Phenogenetic drift in evolution: the changing genetic basis of vertebrate teeth. Proceedings of the National Academy of Science 102, 18063-18068.
Kendall, C., Coplen, T.B., 2001. Distribution of oxygen-18 and deuterium in river waters across the United States. Hydrological Processes 15, 1363-1393.
Klaassen, H.E., Morgan, K.L., 1974. Age and Growth of Longnose Gar in Tuttle Creek Reservoir, Kansas. Transactions of the American Fisheries Society 103, 402-405.
Koch, P.L., Tuross, N., Fogel, M., 1997. The Effects of Sample Treatment and Diagenesis on the Isotopic Integrity of Carbonate in Biogenic Hydroxylapatite. Journal of Archaeological Science 24, 417-429.
Kohn, M.J., Cerling, T.E., 2002. Stable Isotope Compositions of Biological Apatite, in: Kohn, M.J., Rakovan, J., Hughes, J.M. (Eds.), Reviews in Mineralogy & Geochemistry, pp. 455-488.
Kohn, M.J., Schoeninger, M.J., Valley, J.W., 1996. Herbivore tooth oxygen isotope compositions: Effects of diet and physiology. Geochimica et Cosmochimica Acta 60, 3889-3896.
Kolodny, Y., Luz, B., 1991. Oxygen isotopes in phosphates of fossil fish - Devonian to Recent, in: H.P. Tayor, H.P., O'Neil, J.R., Kaplan, I.R. (Eds.), Stable Isotope Geochemistry: A Tribute to Samuel Epstein. Geochemical Society Special Publications, pp. 105-119.
Kolodny, Y., Luz, B., Navon, O., 1983. Oxygen isotope variations in phosphate of biogenic apatites, I. Fish bone apatite - rechecking the rules of the game. Earth and Planetary Science Letters 64, 398-404.
Lécuyer, C., Grandjean, P., Sheppard, S.M.F., 1999. Oxygen isotope exchange between dissolved phosphate and water and temperatures ≤135 °C: Inorganic versus biological fractionations. Geochimica et Cosmochimica Acta 63, 855-862.
LeGrande, A.N., Schmidt, G.A., 2006. Global gridded data set of the oxygen isotopic composition in seawater. Geophysical Research Letters 33, 1-5.
Leng, M.J., Marshall, J.D., 2004. Palaeoclimate interpretation of stable isotope data from lake sediment archives. Quaternary Science Reviews 23, 811-831.
Levinson, A.A., Luz, B., Kolodny, Y., 1987. Variations in oxygen isotopic compositions of human teeth and urinary stones. Applied Geochemistry 2, 367-371.
Liang, Y., 2005. Oxygen Isotope Studies of Biogeochemical Cycling of Phosphorus, Geology & Geophysics. Yale University.
Liang, Y., Blake, R.E., 2006. Oxygen isotope composition of phosphate in organic compounds: isotope effects of extraction methods. Organic Geochemistry 37, 1263-1277.
Longinelli, A., 1966. Ratios of Oxygen-18: Oxygen-16 in phosphate and carbonate from living and fossil marine organisms. Nature 211, 923–927.

Longinelli, A., 1984. Oxygen isotopes in mammal bone phosphate: A new tool for paleohydrological and paleoclimatological research? Geochimica et Cosmochimica Acta 48, 385-390.
Longinelli, A., Nuti, S., 1973a. Oxygen isotope measurements of phosphate from fish teeth and bones. Earth and Planetary Science Letters 20, 337-340.
Longinelli, A., Nuti, S., 1973b. Revised Phosphate-Water Isotopic Temperature Scale. Earth and Planetary Science Letters 19, 373-376.
Love, J.W., 2003. Age, Growth, and Reproduction of Spotted Gar, Lepisosteus oculatus (Lepisosteidae), from the Lake Ponchartrain Estuary, Louisiana. The Southwestern Naturalist 49, 18-23.
Luz, B., Cormie, A.B., Schwarcz, H.P., 1990. Oxygen Isotope variations in phosphate of deer bones. Geochimica et Cosmochimica Acta 54, 1723-1728.
Luz, B., Kolodny, Y., Horowitz, M., 1984. Fractionation of oxygen isotopes between mammalian bone-phosphate and environmental drinking water. Geochimica et Cosmochimica Acta 48, 1689-1693.
McGrath, P., 2010. The Life History of Longnose Gar, *Lepisosteus osseus*, an Apex Predator in the Tidal Waters of Virginia, School of Marine Science. The College of William and Mary, p. 177.
National Centers for Environmental Information, 2022. Climate Data Online. NOAA.
Navarro, N., Lécuyer, C., Montuire, S., Langlois, C., Martineau, F., 2004. Oxygen isotope compositions of phosphate from arvicoline teeth and Quaternary climatic changes, Gingy, French Jura. Quaternary Research 62.
Netsch, N., Witt, A., 1962. Contributions to the Life History of the Longnose Gar, (*Lepisosteus osseus*) in Missouri. Transactions of the American Fisheries Society 91, 251-262.
O'Neil, J.R., Roe, L.J., Reinhard, E., Blake, R.E., 1994. A rapid and precise method of oxygen isotope analysis of biogenic phosphate. Israel Journal of Earth Sciences 43, 203-212.
Pucéat, E., Joachimski, M.M., Bouilloux, A., Monna, F., Bonin, A., Motreuil, S., Morinière, P., Hénard, S., Mourin, J., Dera, G., Quesne, D., 2010. Revised phosphate–water fractionation equation reassessing paleotemperatures derived from biogenic apatite. Earth and Planetary Science Letters 298, 135-142.
Richter, M., Smith, M.F.L.S., 1995. A microstructural study of the ganoine tissue of selected lower vertebrates. Zoological Journal of the Linnean Society 114, 173-212.
Sakaris, P.C., Ferrara, A.M., Kleiner, K.J., Irwin, E.R., 2003. Movements and home ranges of alligator gar in the Mobile-Tensaw Delta, Alabama, Proceedings of the Annual Conference Southeastern Association of Fish and Wildlife Agencies, pp. 102-111.
Sasagawa, I., Ishiyama, M., Yokosuka, H., Mikami, M., 2013. Teeth and ganoid scales in *Polypterus* and *Lepisosteus*, the basic actinopterygian fish: an approach to understand the origin of tooth enamel. Journal of Oral Biosciences 55, 76-84.
Sasagawa, I., Ishiyama, M., Yokosuka, H., Mikami, M., Shimokawa, H., Uchida, T., 2014. Immunohistochemical and Western blot analyses of collar enamel in the jaw teeth of gars, Lepisosteus oculatus, an actinoipterygian fish. Connective Tissue Research 55, 225-233.
Sasagawa, I., Ishiyama, M., Yokosuka, H., Mikami, M., Uchida, T., 2009. Tooth enamel and enameloid in actinopterygian fish. Frontiers of Material Science in China 3, 174-182.

Seal II, R.R., Shanks III, W.C., 1998. Oxygen and hydrogen isotope systematics of Lake Baikal, Siberia: Implications for paleoclimate studies. Limnology and Oceanography 43, 1251-1261.

Simmer, J.P., Fincham, A.G., 1996. Molecular mechanisms of dental enamel formation. Critical Reviews of Oral Biology and Medicine 6, 84-108.

Sire, J.Y., Géraudie, J., Meunier, F.J., Zylberberg, L., 1987. On the origin of ganoine: histological and ultrastructural data on the experimental regeneration of the scales of *Calamoichthys calabaricus* (Osteichthys, Brachyopterygii, Polypteridae). The American Journal of Anatomy 180.

Slater, C., Preston, T., Weaver, L.T., 2001. Stable isotopes and the international system of units. Rapid Communications in Mass Spectrometry 15, 1270-1273.

Smylie, M., Shervette, V., McDonough, C., 2016. Age, Growth, and Reproduction in Two Coastal Populations of Longnose Gars. Transactions of the American Fisheries Society 145, 1.

Snedden, G.A., Kelso, W.E., Rutherford, A.D., 1999. Diel and Seasonal Patterns of Spotted Gar Movement and Habitat Use in the Lower Atchafalaya River Basin, Louisiana. Transactions of the American Fisheries Society 128.

Solomon, D.R., 2012. Life history, growth, and genetic diversity of the spotted gar *Lepisosteus oculatus* from peripheral and core populations, Natural Resources and Environment. University of Michigan, p. 171.

Thomson, K.S., McCune, A.R., 1984. Scale Structure as Evidence of Growth Patterns in Fossil Semionotid Fishes. Journal of Vertebrate Paleontology 4, 422-429.

Tudge, A.P., 1960. A method of analysis of oxygen isotopes in orthophosphate - its use in the measurement of paleotemperatures. Geochimica et Cosmochimica Acta 18, 81-93.

Vennemann, T.W., Fricke, H.C., Blake, R.E., O'Neil, J.R., Colman, A., 2002. Oxygen isotope analysis of phosphates: a comparison of techniques for analysis of Ag_3PO_4. Chemical Geology 185, 321-336.

Wright, J.J., David, S.R., Near, T.J., 2012. Gene trees, species trees, and morphology converge on a similar phylogeny of living gars (Actinopterygii: Holostei: Lepisosteidae), an ancient clade of ray-finned fishes. Molecular Phylogenetics and Evolution 63, 848-856.

Zaarur, S., Affek, H.P., Brandon, M.T., 2013. A revised calibration of the clumped isotope thermometer. Earth and Planetary Science Letters 382, 47-57.

Zaarur, S., Affek, H.P., Stein, M., 2016. Last glacial-Holocene temperatures and hydrology of the Sea of Galilee and Hula Valley from clumped isotopes in *Melanopsis* shells. Geochimica et Cosmochimica Acta 179, 142-155.

Tables and Figures

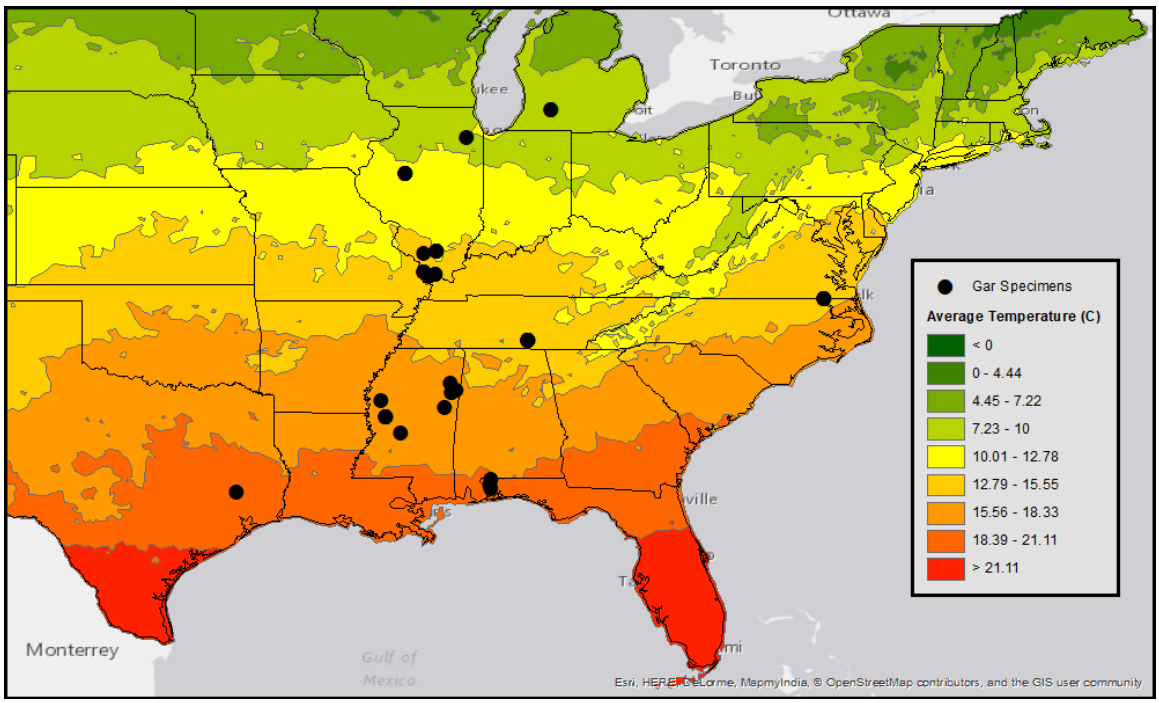

Figure 1. Map of specimen localities superimposed on a map of mean annual air temperature (MAT) (°C) for the continental United States.

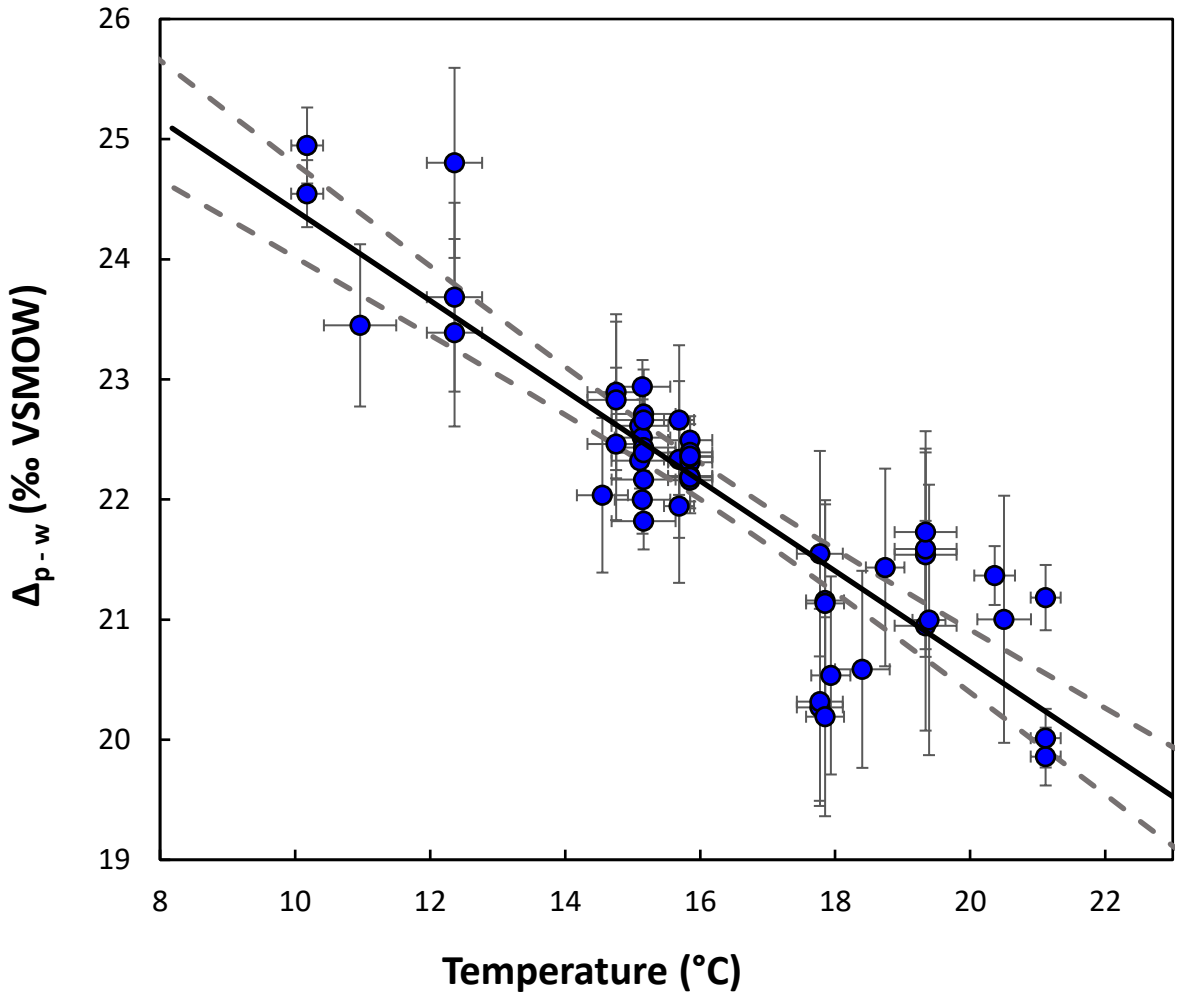

Figure 2. Δ_{P-W} – T calibration line (solid black line) from oxygen-phosphate isotopes in gar scales ($\delta^{18}O_p$) collected from river water with known oxygen isotopic compositions ($\delta^{18}O_w$) (collectively $\delta^{18}O_p$ - $\delta^{18}O_w$ or Δ_{P-W}), and temperature (T, °C). Error bars are 2σ.

769 The dashed gray curves are the 95% confidence interval for the calibration line. Temperatures
770 are mean annual water averages over the lifespan of the gar specimens, approximately fourteen
771 to fifteen years. $\delta^{18}O_w$ are three- to four-year averages (Kendall and Coplen, 2001).

772

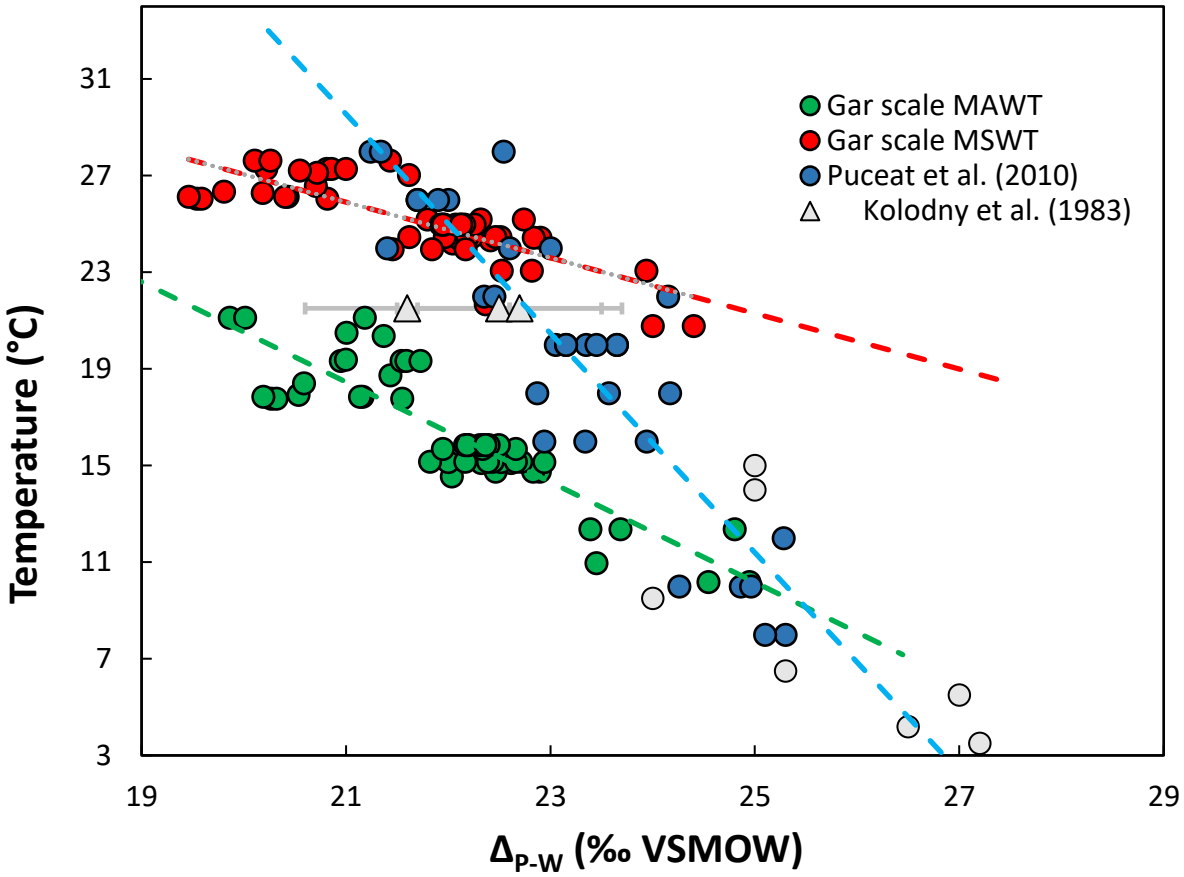

Figure 3. Data from this study (red and green circles) is compared to the values obtained by Pucéat et al. (2010) in their sea bream tank experiment (blue circles). Temperatures used are both mean annual water (green) and mean summer water (red). Gray triangles are from Kolodny et al. (1983), corrected by 2.1 ‰ to account for differences in lab methodology as outlined in Pucéat et al. (2010). Gray triangles and error bars are associated with Lake Kinneret (Sea of Galilee) samples. See section 4.2.

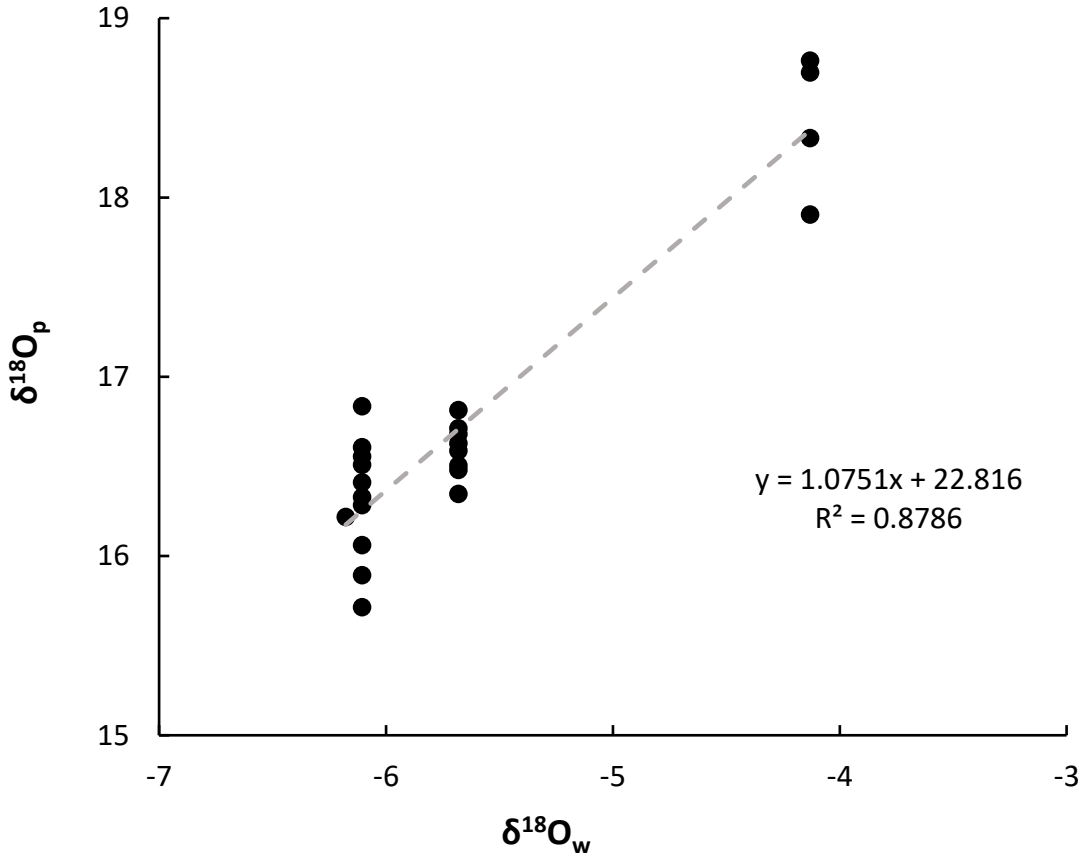

Figure 4. Comparison between $\delta^{18}O_{water}$ and $\delta^{18}O_{phosphate}$ when mean annual water temperature is held constant at ~24.7°C, showing essentially a 1:1 ratio; values are from three different sites; Estill Springs, TN; Ullin, IL; and Peoria, IL.

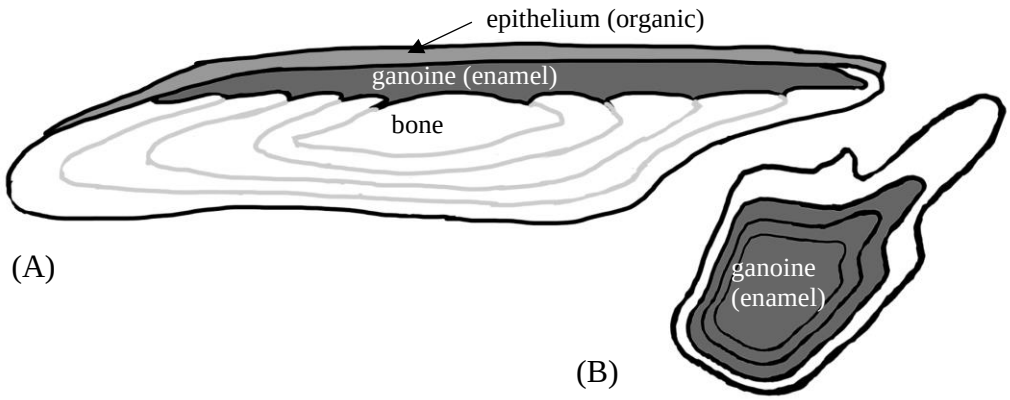

Figure 5. (A) Drawing of a cross section of a gar scale. Ganoine (enamel) directly overlies bone. Banding is seen in the bone with corresponding ridges in the ganoine. In vivo, an organic epithelium covers the scale, giving it color and pattern. (B) One of the three, and most common types of scales seen in gar fish, the dermal scale. Ganoine layering begins in the center (oldest) and extends outwards (youngest). Layering is for illustrative purposes only as banding is most prominent in the bone, not the enamel, and does not represent seasonal growth.

806 **Table 1.** Oxygen isotope values of gar scales. $\delta^{18}O_p$ is averaged from four replicates. $\delta^{18}O_w$ are

807 from USGS measurements (Kendall and Coplen, 2001); see Table S2 for water isotope stations.

Specimen Name	Annual Temperature (°C)	$\delta^{18}O_p$ (‰SMOW)	1 σ	Annual $\delta^{18}O_w$ (‰SMOW)	Δ_{P-W} (‰SMOW)
YPM 12016	9.15± 0.45	16.60	0.19	-7.94	24.55
YPM 8878		17.00	0.21		24.81
FMNH 85897	9.94± 0.82	16.53	0.33	-6.92	23.45
YPM 27219	11.35± 0.74	15.84	0.09	-7.55	23.39
YPM 27220		17.26	0.24		24.80
YPM 27221		16.14	0.18		23.68
YPM 27211	13.77± 0.77	18.76	0.23	-4.13	22.89
YPM 27212		18.33	0.03		22.83
YPM 27216		18.70	0.26		22.46
UF 129480	13.57± 0.72	17.90	0.19	-4.13	22.04
IC-05-01	14.17± 0.74	16.83	0.09	-6.10	22.94
IC-05-02		15.89	0.31		22.00
IC-05-03		16.41	0.39		22.52
ADY-01-01	14.13± 0.76	16.22	0.14	-6.10	22.32
ADY-01-02		16.51	0.36		22.61
IX-03-01	14.17± 0.74	16.33	0.19	-6.10	22.43
IX-03-05		15.71	0.16		21.82
IX-03-06		16.61	0.28		22.71
IX-03-09		16.06	0.06		22.17
IX-03-10		16.56	0.61		22.66
IX-03-11		16.28	0.13		22.39
YPM 11983	14.71± 0.44	17.44	0.33	-4.89	22.33
YPM 12006		17.06	0.26		21.95
YPM 12007		17.77	0.07		22.66
YPM 027686	14.92± 0.59	16.63	0.06	-5.68	22.31
YPM 027687		16.52	0.51		22.03
YPM 027688		16.67	0.19		22.27
YPM 027689		16.81	0.23		22.49
YPM 027690		16.48	0.17		22.16
YPM 027691		16.71	0.31		22.39
YPM 027692		16.50	0.44		22.19
YPM 027693		16.68	0.18		22.36
MMNS 59029	17.16 ± 0.21	17.23	0.14	-3.91	21.13
YPM 27218		16.36	0.05	-3.91	20.27
YPM 27223		17.64	0.41		21.55
YPM 27224		16.41	0.16		20.32
MMNS 51497	17.29 ± 0.31	16.63	0.15	-3.91	20.37
MMNS 58721	17.16 ± 0.21	16.29	0.19	-3.91	20.19
MMNS 58880	17.16 ± 0.21	17.25	0.26	-3.91	21.16
CFM 109203	17.87 ± 0.54	17.53	0.12	-3.91	21.43
MMNS 54500	17.82 ± 0.68	16.68	0.04	-3.91	20.61
MDF 1	18.40 ± 0.84	17.64	0.38	-3.64	21.54

MDF 2		17.68	0.26		21.59
MDF 3	18.40 ± 0.84	17.82	0.31	-3.64	21.73
MDF 4		17.04	0.50		20.95
BARNRES	18.45 ± 0.45	18.23	0.64	-2.77	21.00
UF 120183	19.44 ± 0.55	17.47	0.13	-3.90	21.45
UF 119897	20.20 ± 0.42	15.96	0.15	-3.90	20.96
UF 119908	20.20 ± 0.42	17.28	0.23	-3.90	21.27
UF 150169	19.83 ± 0.66	16.11	0.21	-3.90	19.43
TNSC 31670	19.39 ± 0.75	17.19	0.64	-3.81	21.00

Supplementary Material

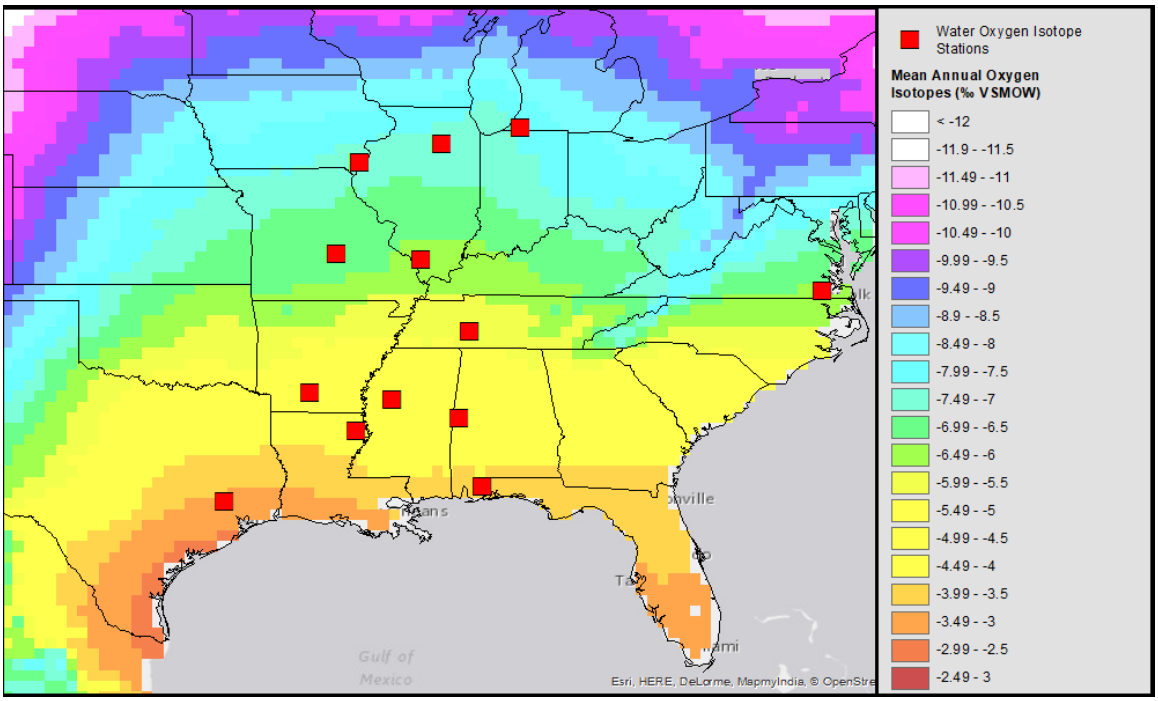

Figure S1. Map of water station localities (IAEA/WMO, 2018) superimposed on a map of mean annual oxygen isotopes $\delta^{18}O_{water}$ for the continental United States (Bowen and Revenaugh, 2003; Bowen et al., 2005).

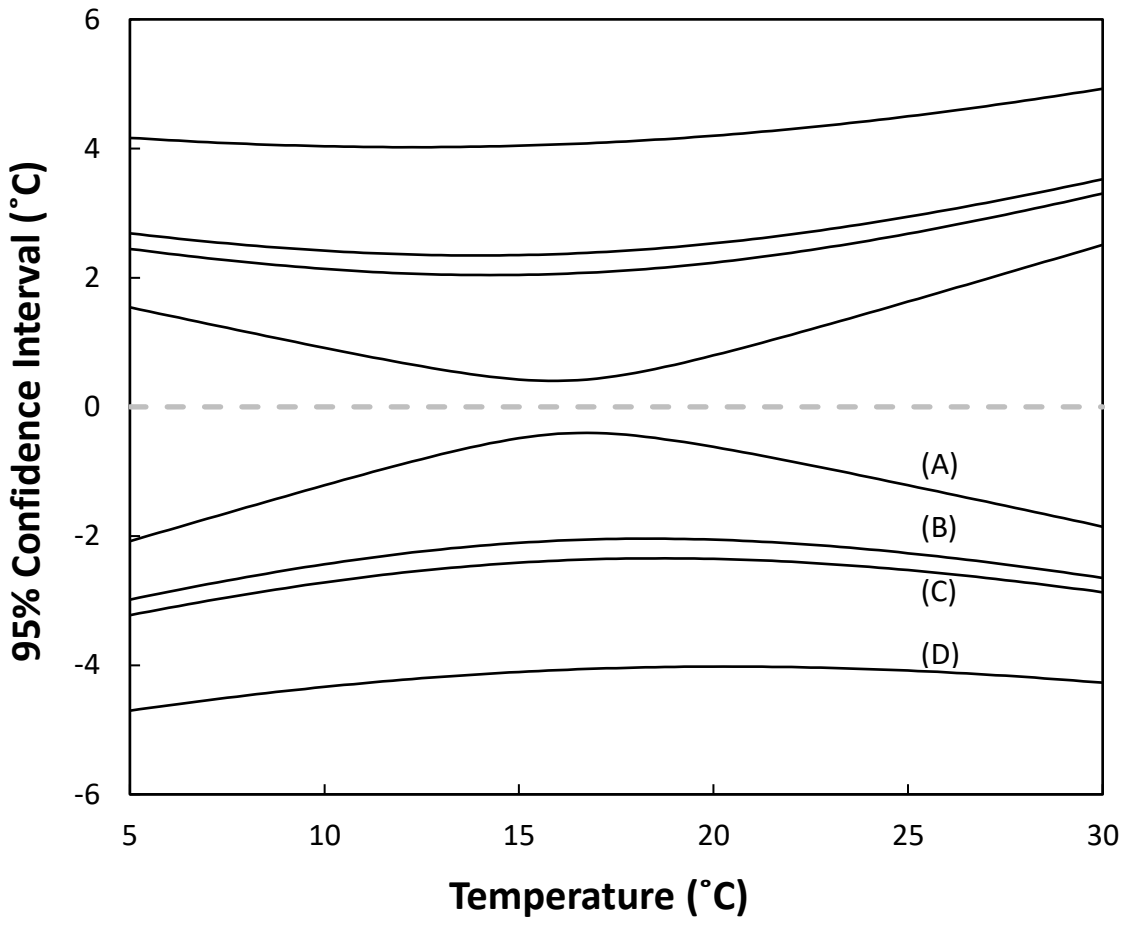

Figure S2. Graphic summary of 95% uncertainty for a temperature estimated using the gar scale bioapatite calibration. Uncertainty is a function of temperature and standard error contours. Maximizing numbers of unique sites (n_s) with multiple fish specimens (n_r) with multiple replicates of $\delta^{18}O_p$ reduces SE(Δ_{P-W}). (A) Uncertainty comes from the calibration error alone, with SE (Δ_{P-W}) = 0‰. (B) SE = 0.371‰, $n_s = n_r = 4$. This is closest to the average number of sites and number of fish specimens in this study. (C) SE = 0.428‰, $n_s = n_r = 3$. (D) SE = 0.742‰, $n_s = n_r = 1$.

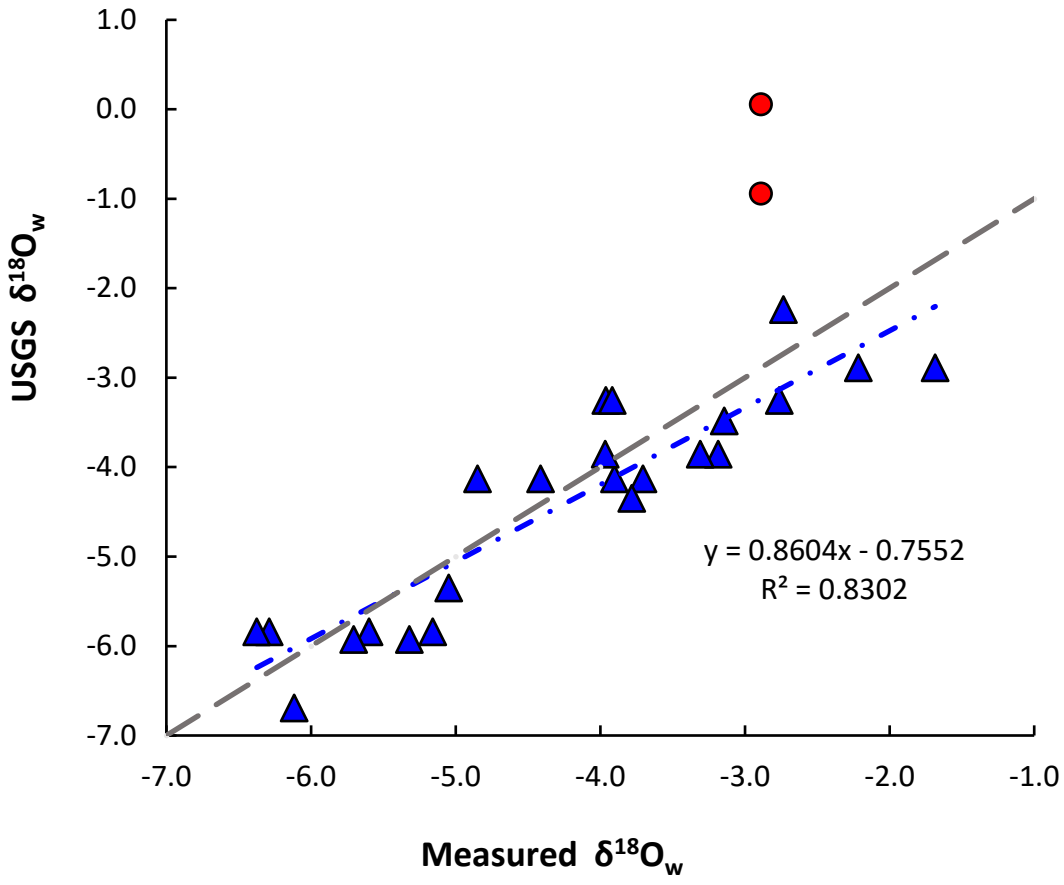

Figure S3. $\delta^{18}O_{water}$ values from waters collected in July 2014 compared to summer (July and August) values from those collected by the USGS from 1984 to 1987 (Kendall and Coplen, 2001). Two outliers (red circles) were collected on 19 July 2014 from east Texas after heavy rainfall (~50 mm) following mild drought conditions. Gray dashed line is 1:1 relationship. These values and their constituent samples were ultimately not included in this phosphate-oxygen isotope dataset.

Table S1. Specimen localities and annual water oxygen isotope compositions**.** $\delta^{18}O_{water}$ measurements are from USGS measurements (Kendall and Coplen, 2001). Annual air temperature are average temperatures taken from NOAA's National Centers for Environmental Information. Abbreviations: Yale Peabody Museum (YPM); Florida Museum of Natural History (UF); Texas Natural Science Center (TNSC); Chicago Field Museum (FMNH).

Specimen Name	Coordinates	Location	Annual Air Temp (°C)	Annual $\delta^{18}O_{water}$ (‰SMOW)	$\delta^{18}O_w$ Measurement Location
YPM 12016 YPM 8878	42.399700°N, 85.411400°W	Gull Lake, MI	9.15 ± 0.45	-7.94	St. Joseph River, Niles, MI
FMNH 85897	41.530978°N, 88.032708°W	Joliet, IL	9.94 ± 0.82	-6.92	Illinois River, Marseilles, IL
YPM 27220 YPM 27221 YPM 27222	40.445169°N, 89.948581°W	Canton, IL	11.35 ± 0.74	-7.55	Skunk River, Augusta, IA
YPM 27211 YPM 27212 YPM 27216	38.037086°N, 88.956222°W	Rend Lake Dam, IL	13.77 ± 0.77	-4.13	Big Muddy River, Murphys-boro, IL
UF 129480	37.967501°N, 89.351882°W	Du Quoin, IL	13.57 ± 0.72	-4.13	Big Muddy River, Murphys-boro, IL
IC-05-01 IC-05-02 IC-05-03	37.368500°N, 89.360119°W	McLure, IL	14.17 ± 0.74	-6.10	Gasconade River, Jerome, MO
ADY-01-01 ADY-01-02	37.306750°N, 88.984069°W	Karnak, IL	14.13 ± 0.76	-6.10	Gasconade River, Jerome, MO
IX-03-01 IX-03-05 IX-03-06 IX-03-09 IX-03-10 IX-03-11	37.273281°N, 89.183789°W	McLure, IL	14.18 ± 0.86	-6.10	Gasconade River, Jerome, MO
YPM 11983 YPM 12006 YPM 12007	36.546089°N, 76.931078°W	Holland, VA	14.71 ± 0.44	-4.89	Blackwater River, Franklin, VA
YPM 027686 YPM 027687 YPM 027688 YPM 027689	35.255697°N, 86.133170°W	Estill Springs, TN	14.88 ± 0.60	-5.68	Buffalo River, Flat Woods, TN

YPM 027690 YPM 027691 YPM 027692 YPM 027693					
MMNS 59029	33.936869°N, 88.531789°W	Aberdeen, MS	16.90 ± 0.53	-3.91	Yazoo River, Shell Bluff, MS
YPM 27218 YPM 27223 YPM 27224	33.808794°N, 88.774011°W	Grenada, MS	16.82 ± 0.62	-3.91	Yazoo River, Shell Bluff, MS
MMNS 51497	33.705806°N, 88.343700°W	Hamilton, MS	16.98 ± 0.55	-3.91	Yazoo River, Shell Bluff, MS
MMNS 58721	33.662754°N, 88.501777°W	West Point, MS	16.90 ± 0.53	-3.91	Yazoo River, Shell Bluff, MS
MMNS 58880	33.636978°N, 88.501311°W	West Point, MS	16.90 ± 0.53	-3.91	Yazoo River, Shell Bluff, MS
FMNH 109203	33.398444°N, 90.700560°W	Indianola, MS	17.80 ± 0.54	-3.91	Yazoo River, Shell Bluff, MS
MMNS 54500	33.189222°N, 88.708694°W	Brooksville, MS	17.46 ± 0.74	-3.91	Yazoo River, Shell Bluff, MS
MDF 3	32.897717°N, 90.537892°W	Yazoo City, MS	18.40 ± 0.84	-3.64	Wolf River, Landon, MS
MDF 4 MDF 1 MDF 2	32.896631°N, 90.541906°W	Yazoo City, MS	18.40 ± 0.84	-3.64	Wolf River, Landon, MS
BARNRES	32.395362°N, 90.066850°W	Jackson. MS	18.45 ± 0.45	-2.77	Tensas River, Tendal, LA
UF 120183	30.947522°N, 87.263955°W	Jay, FL	19.44 ± 0.55	-3.90	Perdido River, Barrineau, AL
UF 119897	30.775972°N, 87.309028°W	Molino, FL	20.20 ± 0.42	-3.90	Perdido River, Barrineau, AL
UF 119908	30.679889°N, 87.268861°W	Molino, FL	20.20 ± 0.42	-3.90	Perdido River, Barrineau, AL
UF 150169	30.775833°N, 87.339167°W	Molino, FL	20.20 ± 0.42	-3.90	Perdido River, Barrineau, AL
TNSC 31670	30.555314°N, 95.185664°W	Coldspring, TX	19.39 ± 0.75	-3.81	San Jacinto, Conroe, TX

Table S2. Summer only $\delta^{18}O_{water}$ average values (July and August) of the water isotope stations monitored by the USGS from 1984 to 1987 (Kendall and Coplen, 2001) compared to $\delta^{18}O_{water}$ values from waters collected in July 2014. FMNH = Chicago Field Museum, TNSC = Texas Natural Science Center, UF = Florida Museum of Natural History, YPM = Yale Peabody Museum.

Location or Catalog Number	City, State	Coordinates	Date Sampled	Sampled $\delta^{18}O_{water}$	Station $\delta^{18}O_{water}$	River Station Name
Presque Isle	Erie, PA	42.160010°N, 80.094269°W	04-Jul-14	-6.12	-6.69	Grand, Painesville, OH
FMNH 85897	Joliet, IL	41.530978°N, 88.032708°W	07-Jul-14	-5.60	-5.84	Illinois, Marseilles, IL
FMNH 124364	Channahon, IL	41.401133°N, 88.280402°W	07-Jul-14	-6.29	-5.84	Illinois, Marseilles, IL
FMNH 11168	Dayton, IL	41.386380°N, 88.789155°W	07-Jul-14	-6.37	-5.84	Illinois, Marseilles, IL
Rice Lake	Banner, IL	40.480604°N, 89.939408°W	08-Jul-18	-5.16	-5.84	Illinois, Marseilles, IL
Pere Marquette State Park	Grafton, IL	38.971261°N, 90.545534°W	09-Jul-18	-5.32	-5.93	Salt, New London, MO
FMNH 83724	Grafton, IL	38.968445°N, 90.438492°W	09-Jul-18	-5.70	-5.93	Salt, New London, MO
Rend Lake Dam	Benton, IL	38.037437°N, 88.956454°W	10-Jul-18	-4.41	-4.13	Big Muddy River, Murphysboro, IL
Clear Creek	McLure, IL	37.368500°N, 89.360119°W	21-Jul-14	-3.90	-4.13	Big Muddy River, Murphysboro, IL
Old Cache River	Karnak, IL	37.306750°N, 88.984069°W	21-Jul-14	-3.71	-4.13	Big Muddy River, Murphysboro, IL
Cache River	Ullin, IL	37.273281°N, 89.183789°W	17-Jul-14	-4.85	-4.13	Big Muddy River, Murphysboro, IL
Nottoway River	Holland, VA	36.546089°N, 76.931078°W	28-Jul-14	-3.78	-4.35	Blackwater, Franklin, VA
Henry Horton State Park	Wilhoite Mills, TN	35.590478°N, 86.700220°W	14-Jul-14	-5.05	-5.35	Buffalo, Flat Hills, TN
YPM 27218	Grenada Dam, MS	33.808794°N, 89.774011°W	15-Jul-14	-3.96	-3.25	Yazoo, Shell Bluff, MS
MMNS 58721	Barton Ferry, MS	33.664683°N, 88.501955°W	15-Jul-14	-3.92	-3.25	Yazoo, Shell Bluff, MS
Sunflower River, MS	Indianola, MS	33.398444°N, 90.700560°W	16-Jul-14	-2.76	-3.25	Yazoo, Shell Bluff, MS
Barnet Reservoir	Jackson, MS	32.395362°N, 90.066850°W	17-Jul-14	-2.73	-2.24	Tensas, Tendal, LA
UF 120183	Jay, FL	30.947522°N, 87.263955°W	26-Jul-14	-3.18	-3.86	Perdido, Barrineau Park, AL

UF 119897	Molino, FL	30.775972°N, 87.309028°W	26-Jul-14	-3.97	-3.86	Perdido, Barrineau Park, AL
UF 119908	Pensacola, FL	30.679889°N, 87.268861°W	26-Jul-14	-3.31	-3.86	Perdido, Barrineau Park, AL
Lake Livingston, TX	West Livingston, TX	30.631787°N, 95.010855°W	25-Jul-14	-1.68	-2.89	West Fork San Jacinto, Conroe, TX
TNHC 48690	Bryan, TX	30.559488°N, 96.423447°W	19-Jul-14	-2.22	-2.89	West Fork San Jacinto, Conroe, TX
TNHC 46355	Hutto, TX	30.526316°N, 97.566827°W	19-Jul-14	-3.14	-3.48	South Fork Rocky Creek, Briggs, TX
TNHC 58066	Clay, TX	30.368110°N, 96.343175°W	19-Jul-14	0.06	-2.89	West Fork San Jacinto, Conroe, TX
TNHC 15583	Hempsted, TX	30.097696°N, 96.158949°W	19-Jul-14	-0.94	-2.89	West Fork San Jacinto, Conroe, TX

References

Bowen, G.J., Revenaugh, J., 2003. Interpolating the isotopic composition of modern meteoric precipitation. Water Resources Research 39, 1299.

Bowen, G.J., Wassenaar, L.I., Hobson, K.A., 2005. Global application of stable hydrogen and oxygen isotopes to wildlife forensics. Oecologia 143, 337-348.

IAEA/WMO, 2018. Global Network of Isotopes in Precipitation. The GNIP Database.

Kendall, C., Coplen, T.B., 2001. Distribution of oxygen-18 and deuterium in river waters across the United States. Hydrological Processes 15, 1363-1393.